PAPER

Comparison of different kinetic models for dynamic ^{18}F-FDG PET/CT imaging of hepatocellular carcinoma with various, also dual-blood input function

IOP Publishing Phys. Med. Biol. 65 (2020) 045001 (9pp) https://doi.org/10.1088/1361-6560/ab66e3

Physics in Medicine & Biology

IPEM Institute of Physics and Engineering in Medicine

PAPER

RECEIVED
17 September 2019

REVISED
17 December 2019

ACCEPTED FOR PUBLICATION
2 January 2020

PUBLISHED
10 February 2020

Comparison of different kinetic models for dynamic ^{18}F-FDG PET/CT imaging of hepatocellular carcinoma with various, also dual-blood input function

Barbara Katharina Geist[3,6], Jingnan Wang[1,2,6], Xuezhu Wang[1,2], Jianzhen Lin[4], Xu Yang[4], Hui Zhang[5], Fang Li[1,2], Haitao Zhao[4], Marcus Hacker[3], Li Huo[1,2,7] and Xiang Li[3]

[1] Department of Nuclear Medicine, Chinese Academy of Medical Sciences and Peking Union Medical College Hospital, Beijing, People's Republic of China
[2] Beijing Key Laboratory of Molecular Targeted Diagnosis and Therapy in Nuclear Medicine, Chinese Academy of Medical Sciences and Peking Union Medical College Hospital, Beijing, People's Republic of China
[3] Division of Nuclear Medicine, Department of Biomedical Imaging and Image-guided Therapy, Medical University of Vienna, Vienna, Austria
[4] Department of Liver Surgery, Chinese Academy of Medical Sciences and Peking Union Medical College Hospital, Beijing, People's Republic of China
[5] Department of Biomedical Engineering, Tsinghua University, Beijing, People's Republic of China
[6] Both authors contributed equally to this work.
[7] Author to whom any correspondence should be addressed.

E-mail: HuoLi@pumch.cn

Keywords: FDG, positron emission tomography, hepatocellular carcinoma, dual input function, kinetic model

Abstract

A kinetic modeling analysis was performed on hepatocellular carcinoma (HCC) as well as healthy liver tissue regions from dynamic FDG positron emission tomographys/computer tomography (PET/CT) cans. On basis of image derived input function from hepatic artery and portal vein, various kinetic models were compared among each other in order to check whether HCC can be classified and differ from healthy tissue within the kinetic parameters.

14 HCC and 10 healthy liver regions from FDG PET/CT scans of ten patients were analyzed from their time activity curves (TACs) were extracted from the PET dynamic images. Also the hepatic artery and the portal vein were delineated in the fused PET/CT images, which were used as input functions. Four kinetic models were applied to the TACs, using both or only one input function. Results were analyzed with several information criteria according to Akaike and Schwartz as well as be the F-Test. The paired student's *t*-test was used to determine the differences between HCC and healthy regions.

All applied models revealed significant differences of $p < 0.01$ of k_3 between HCC and healthy liver and three out of four models produced almost identical values for $k_3 = 0.03\,\mathrm{min}^{-1}$ and $K_i = 0.03\,\mathrm{min}^{-1}$. According to the information criteria tests, a simple two-tissue model with only a venous input function is clearly preferred in case of HCC TACs. After dividing all HCC regions into two groups having a low and a high HCC-to-healthy ratio, respectively, this model also showed significant differences of k_3 between these two groups.

In conclusion, results indicate that the portal vein is sufficient to describe kinetic FDG processes in HCC and healthy liver regions.

Introduction

Hepatocellular carcinoma (HCC) is the fifth leading cause of cancer related deaths with an increasing incidence in East Asia and Western Europe (Akinyemiju and Global Burden of Disease Liver Cancer Collaboration 2017, Siegel *et al* 2018). Due to the hidden onset and lack of effective biomarkers, most cases are already advanced at the

time of diagnosis. Therefore, HCC remains an important global clinical challenge (Margini and Dufour 2016). Strategies based on a personal need to treat HCC using combination therapies including immune checkpoint inhibitors, chemotherapy, transarterial chemoembolization and radiofrequency ablation (Heimbach *et al* 2018, El Dika *et al* 2019). Although limited sensitivity has been considered using [^{18}F] fluorodeoxyglucose ([^{18}F]-FDG) positron emission tomography (PET) in HCC (Ho *et al* 2003), it is an effective non-invasive imaging method to detect unexpected intra- and extra-hepatic metastasis, evaluate biological activity, predict recurrence pattern and aid the selection of treatment for HCC (Li *et al* 2017, Lee *et al* 2019). Qualitative or quantitative parameters are mainly evaluated on static imaging. However, as an imaging marker for glucose metabolism, the dynamic FDG PET with kinetic modeling of this metabolic process has not been established clearly. Limited studies have reported that dynamic FDG PET with kinetic modeling is promising in the differential diagnosis and therapeutic assessment in HCC (Okazumi *et al* 1992, Huo *et al* 2015). Understanding the kinetic behavior of FDG, i.e. describing the processes of FDG mathematically with a compartmental kinetic model, may have potential significance in clinical evaluation for HCC. In this study, we attempt to establish a FDG PET dynamic model in HCC using human patient data for accurate differentiation, therapeutic response prediction and assessment.

A kinetic model in principle is a set of differential equations containing rate constants which allow a quantification of the biochemical processes. For solving the equations in order to obtain the rate constants, an input curve is needed. If not obtained by external arterial blood sampling, the image derived input function (IDIF) can be delineated from an aortic volume (Chen *et al* 1998, Geist *et al* 2018). In the liver both, the hepatic artery as well as the portal vein contribute to the blood supply in the liver (Keiding 2012). Therefore, the tracer concentration of the hepatic artery and the portal vein need to be taken into account to ensure reasonable results. However, the FDG concentration in the portal vein is different from the hepatic artery and it is difficult to obtain (Keiding 2012). Furthermore, due to its position in the human body and its relatively small lumen, motion and partial volume effects, respectively, hamper a proper delineation from dynamic PET scans. To overcome this, the input function from the portal vein is assessed from a metabolic and flow models (Munk *et al* 2001, Kudomi *et al* 2009) or estimated with a compartment model (Wang *et al* 2018).

These methods need many fit parameters and rely on estimations. The objective of this study therefore was to perform a kinetic modeling analysis with two IDIFs from hepatic artery and portal vein and to check, whether a HCC can be classified. For this, HCC regions were compared to healthy liver tissue. Furthermore, several different models considering one or two input functions were compared.

Materials and methods

PET/CT scans were conducted on a PoleStar m660 PET/CT scanner (SinoUnion Healthcare, Beijing, China) at Peking Union Medical College Hospital (PUMCH) (Huo *et al* 2018). The dynamic PET studies were performed over the liver region after intravenous administration of 3.70–5.55 MBq kg^{-1} (0.1–0.15 mCi kg^{-1}) [^{18}F]-FDG for 60 min using a 110-frame sampling protocol (60 frames of 10 s, 50 frames of 60 s). A standard dose CT scan (120 kV, 260 effective mA) was performed for attenuation correction and image fusion. Dynamic PET images were then reconstructed using a manufacturer (SinoUnion Healthcare, Beijing, China) provided stand-alone advanced research workstation with standard ordered subset expectation maximization (OSEM) algorithm with 2 iterations and 10 subsets.

Patient treatment

Ten patients with advanced HCC during the course of any treatment line underwent dynamic 18F-FDG PET/CT were recruited in this study. The pathology of eight patients was confirmed by surgery and the other two was confirmed by needle biopsy. Therapeutic history of these patients included systemic immune checkpoint inhibitors therapy, chemotherapy, local radiotherapy, transarterial chemoembolization and radiofrequency ablation. The use of the patient data was approved by the Ethics Committee at Peking Union Medical College Hospital (JS1964). All patients signed informed consent.

Image analysis

Delineation of volumes of interest were done with the Hermes Hybrid Viewer tool (Hermes Medical Solutions AB, Stockholm, Sweden). In the CT image of each patient, volumes of interest (VOIs) were drawn manually over all visible HCC lesions as well as over an area far away from any lesion, called 'remote'. A VOI was drawn within the hepatic artery (here denoted as A) as well as the portal vein (V). VOIs were copied to the PET images after image fusion; the according concentration time activity curves (TACs) in units of standardized uptake value (SUV) as well as maximum SUV (SUVmax) and the according volume sizes were exported. A representative PET/CT scan is shown in figure 1.

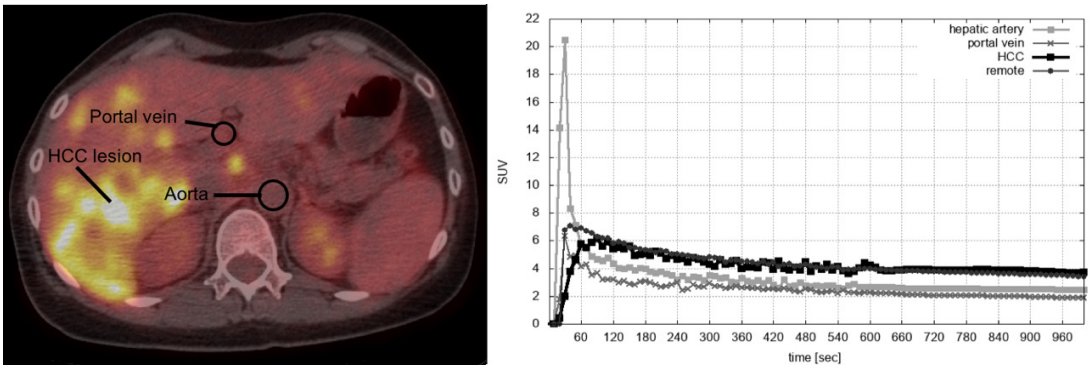

Figure 1. Left: Representative images of a 40-year-old female patient with moderately to poorly differentiated metastatic tumor after combined immune checkpoint inhibitor therapy. Transverse static PET/CT slices show aorta, portal vein and tumor lesions; hepatic artery cannot be seen. Right: Typical time activity curves (TACs) from delineated regions.

Kinetic models

FDG kinetics are usually described with a two-tissue model (Schmidt and Turkheimer 2002) applied to measured TACs (for typical TACs, see figure 1). In the kinetic model, the glucose transport from blood to the hepatic tissue is described via the rate constant K_1 (ml/min/ml) and the opposite direction via k_2 (1/min). The further phosphorylation of FDG by hexokinase into FDG 6-phosphate is represented by another rate constant k_3 (1/min) and the dephosphorylation with k_4 (1/min). These processes underlie the total tissue curve, which is equivalent to the measured remote or HCC TAC in the PET images, denoted as C_{measured}. In the following, $C_1(t)$ represents the free-state FDG concentration in the hepatic tissue compartment, $C_2(t)$ the metabolized FDG 6-phosphate concentration, $A(t)$ the FDG concentration in the hepatic artery and $V(t)$ in the portal vein.

Four models were compared. First, a classic two-tissue model with one input function from the hepatic artery was created (see figure 2, model A). With v_B as the fraction of the measured volume occupied by blood and K_a as K1 arising from $A(t)$, the according equations can be formulated as

$$\frac{dC_1(t)}{dt} = K_A A(t) - (k_2 + k_3) C_1(t) + k_4 C_2(t) \tag{1}$$

$$\frac{dC_2(t)}{dt} = k_3 C_1(t) - k_4 C_2(t) \tag{2}$$

$$C_{measured}(t) = (1 - v_B)(C_1(t) + C_2(t)) + v_B A(t). \tag{3}$$

For model B (figure 2(B)), a second input to compartment $C_1(t)$ coming from the portal vein via K_v was added to the arterial input via K_a. Thus, equation (1) needs to be re-written as:

$$\frac{dC_1(t)}{dt} = K_a A(t) + K_v V(t) - (k_2 + k_3) C_1(t) + k_4 C_z(t) \tag{4}$$

Since $A(t)$ and $V(t)$ are both contributing to the fraction of blood volume, each amount was assessed from their inflow rate constants, equation (3) therefore results in:

$$C_{measured} = (1 - v_B)(C_1(t) + C_2(t)) + v_B \left(A(t) \frac{K_a}{K_a + K_v} + V(t) \frac{K_a}{K_a + K_v} \right). \tag{5}$$

Model C (figure 2(C)) is in principle identical to model A, where the input from the hepatic artery $A(t)$ was replaced by the input from the portal vein $V(t)$. This means, $A(t)$ has to be replaced by $V(t)$ in equations (1) and (3).

As a forth model, the model suggested by Wang *et al*[16] was applied. The first part of the model is a two-tissue model identical to model A, thus equations (1)–(3) were applied. Additionally, in this model the input function itself is assumed to be the result of a one-tissue analysis, therefore $A(t)$ in equation (1) was replaced by a compartment C_{input} using the blood pool B(t) as input:

$$C_{input}(t) = f_A B(t) + (1 - f_A)(k_a e^{-k_a t} \times B(t)). \tag{6}$$

The two additionally needed fit parameters k_a and f_A represent the rate constant and the fraction of hepatic artery contributing to the liver blood flow.

The two input functions, $A(t)$ and $V(t)$ were fitted with a tri-exponential function starting from the peak maximum and with a linear increase before the maximum. With the rate constants as fit parameters, all model fits were performed according to the least-squares method and optimized with a Levenberg–Marquardt

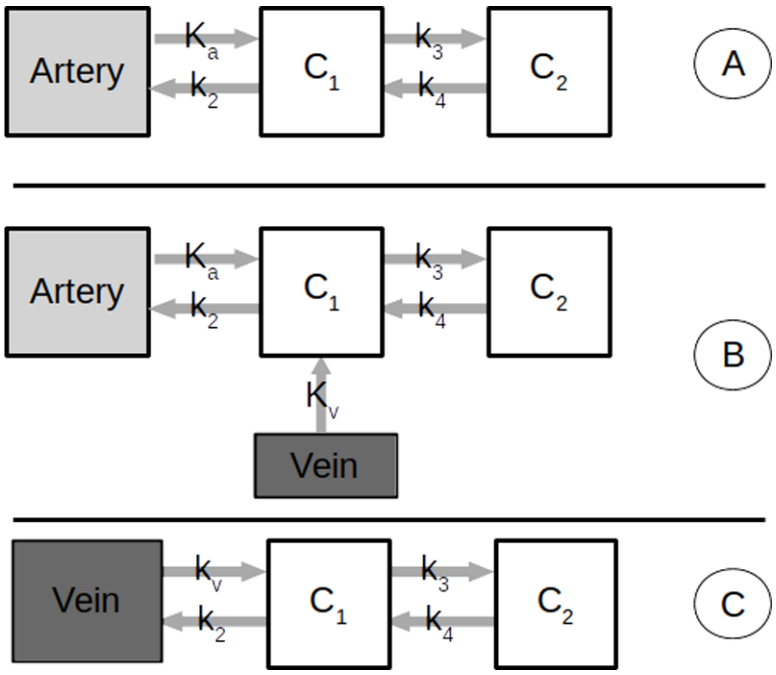

Figure 2. Schematic presentation of three of the four used models. Model A and C are simple two-tissue models with the hepatic artery $A(t)$ and the portal vein $V(t)$ as input function, respectively. In model B, both input functions $A(t)$ and $V(t)$ contribute to the first compartment C_1. A detailed description of the fourth model can be found in Wang's work (Wang *et al* 2018).

algorithm, implemented to a Java program. The uncertainties of the fit parameters were obtained from the calculated covariance matrix. For models A, B and C, the initial parameters were set to $K_A = 0.5\,\text{min}^{-1}$, $K_V = 1.0\,\text{min}^{-1}$, $k_2 = 0.5\,\text{min}^{-1}$, $k_3 = 0.05\,\text{min}^{-1}$, $k_4 = 0.01\,\text{min}^{-1}$ and $v = 0.1$. For the fourth model by Wang *et al*, the initial parameters were chosen according to their reported mean values ($K_1 = 0.98\,\text{min}^{-1}$, $k_2 = 1.1\,\text{min}^{-1}$, $k_3 = 0.01\,\text{min}^{-1}$ and $k_4 = 0.05\,\text{min}^{-1}$, $k_a = 1.9\,\text{min}^{-1}$, $f_A = 0.04$, $v = 0.02$).

In summary, the final analyzed data were, prepared for each VOI: the calculated rate constants including their uncertainties, the residual sum of squares weighted by a factor for time frames (WRSS), the sum of SUVmax over the total TAC, the sum of the SUV of the last 10 min and the size of the volume.

The average and standard deviation of the rate constants, including $K_i = K_1 k_3/(k_2 + k_3)$, was calculated for all HCC well as for all remote TACs.

Statistical analysis

In order to find the optimum model, the four models were compared using the F-Test, Akaike Information Criterion (AIC), AIC unbiased (AICC) and Schwartz Criterion (SC) as suggested by Golla *et al* (2017). These tests were applied to every TAC; the percentage of TACs which showed the minimum value of each test was then calculated.

The paired student's *t*-test was used to assess the significance of the difference in each rate constant *k* between a HCC and its according remote region, as well as between each model.

Results

Ten patients were evaluated. From each patient, one remote liver VOI was taken and at least one HCC VOI. In four patients, a second HCC VOI was delineated (Galle *et al* 2018), leading therefore to altogether 14 HCC TACs and 10 remote TACs.

SUVmax and volumes

A summary of all VOI sizes and SUVmax values is in shown in table 1. Note that only one HCC had size of 1 cm^3, all other VOIs had a size of at least 3 cm^3.

Comparison of kinetic models

The obtained rate constants, averaged for HCC and remote regions separately, are presented in table 2. Also the *p*-values obtained from the student's *t*-test after comparing HCC and remote in each patient are shown,

Table 1. Statistics from all volumes of interests: the size of the volumes (vol) and the sum of the maximum standardized uptake value (SUVmax) relative to healthy liver tissue ('remote') from hepatocellular carcinoma (HCC) to, the hepatic artery (artery) as well as the portal vein (vein). Mean is the mean value, '1 SD%' stands for one standard deviation in percent of the mean value, min for minimum and max for maximum measured value. To make patients comparable among each other, values were normalized on the remote region.

	HCC/remote		Artery /remote		Vein /remote	
	SUV-max	vol [cm^3]	SUV-max	vol [cm^3]	SUV-max	vol [cm^3]
Mean	1.5	9.1	0.7	7.8	0.6	2.9
1 SD%	32%	77%	16%	63%	26%	25%
Min	1.1	1.0	0.5	3.8	0.3	1.7
Max	2.8	23.8	0.9	19.1	0.8	3.8

significant differences ($p < 0.05$) are underlined. In model B, K_A varied in all HCC TACs between 0.00 min^{-1} and 0.62 min^{-1}, K_V between 0.07 min^{-1} and 3.04 min^{-1}.

As presented in figure 3, the results of the criteria tests, AIC (checked pattern), AICC (plane) and SC (striped pattern) are shown for all four models, separately for HCC (figure 3(a)) and remote (figure 3(b)). Model C, i.e. a simple two-tissue model with venous input function, is clearly preferred in case of HCC TACs and Wang's model in case of remote TACs. The F Test showed that model B was better than Wang's model with p-values of less than 0.01 in 50% of all HCC TACs. For remote TACs, Wang's model gave in each comparison a p-value of less than 0.01 for at least 80% of all TACs, showing an unambiguous preference for Wang's model.

Comparing the rate constants of HCC TACs between models A, B and C, the student's t-test showed no significant differences in k_4 and K_i, except for k_4 between model A and model C ($p = 0.03$). Between Wang's model and the others, significant differences were found for k_4 and K_i with p-values between 0.01 and 0.03.

In case of k_3, no significant difference and almost even equal values were found between models A, B and C with p-values between 0.74 and 0.87. Comparing only these three models, the values of k_3 deviate in four TACs with more than 33% from each other, as visible in figure 4. Including Wang's model, values of k_3 deviate in eight TACs with more than 33%. In detail, between model A and Wang's model, a significant difference of k_3 with $p = 0.03$ was found. Between model B and Wang's model, no significant difference was found ($p = 0.20$), also between model C and Wang's model ($p = 0.21$). For model A, k_3 varied between 0.01 min^{-1} and 0.06 min^{-1}, for model B between 0.01 min^{-1} and 0.09 min^{-1}, for model C between 0.00 min^{-1} and 0.10 min^{-1} and for Wang's model between 0.02 min^{-1} and 0.12 min^{-1}. The values of k_3 and K_i are the only ones which show significant differences between HCC and remote region for every model (see table 2).

Classification of HCCs

HCC SUV mean values, calculated from the last 10 min of the scan, were separated into two groups: group 1 with an SUVmean ratio HCC-to-remote of less than 2 ($n = 6$), with an average of 1.6, and group 2 with HCC-to-remote ratio of higher than 2 ($n = 8$) with an average of 2.7. Averaged values for k_3 in group 1 and 2 were (0.02 ± 0.02) min^{-1} and (0.04 ± 0.01) min^{-1} for model A, (0.02 ± 0.02) min^{-1} and (0.05 ± 0.03) min^{-1} for model B, (0.01 ± 0.01) min^{-1} and (0.05 ± 0.03) min^{-1} for model C and finally (0.04 ± 0.0) min^{-1} and (0.05 ± 0.03) min^{-1} for Wang's model, as illustrated in figure 5(A). Model A, B and C showed significant differences in k_3 between these two groups of $p = 0.03$, $p = 0.03$ and $p = 0.01$, respectively. No significant differences were found in K_A for all models. Wang's model showed no significant differences ($p = 0.22$). Also a positive correlation between SUVmean HCC-to-remote ratio and k_3 could be found for all models, as presented in figure 5(B) for models B, C and Wang's model. For model A, a correlation of $r = 0.71$ was found.

Discussion

FDG PET could determine the changes in glucose metabolism. Dynamic FDG PET with kinetic model may provide additional information in assessing tumor viability than traditional static parameters like standard uptake value (SUV). There are few studies using different models to distinguish benign and malignant liver lesions. Since liver has blood supply from both the hepatic artery and portal vein, seeking an accurate input model is important for the following quantitative method in the analysis of liver tumors. In this study, we introduced a FDG dynamic model of liver metabolism and compare the quantitative parameters between tumor lesions and healthy liver regions. The TACs of HCC lesions and healthy liver regions ('remote') were fitted with four models: model A using the hepatic artery as input, model B using both hepatic artery and portal vein, model C using solely the portal vein as input and finally a model designed by Wang *et al* (2018) using a modeled input function. Models were compared with several information criteria and rate constants were compared among the models as well as between healthy liver ('remote') and HCC regions.

Table 2. Results of the four tested models A, B, C and Wang's model (see figure 2) for hepatocellular carcinoma (HCC) and a region of healthy liver tissue (remote). K_a stands for K_1 from the hepatic artery, K_v for K_1 from the portal vein. Values are shown as mean value over all TACs in 1/min plus-minus one standard deviation. Also the p-values from student's t-test after comparing HCC and remote are shown. Significant differences of $p < 0.05$ are underlined.

		K_a	K_v	k_2	k_3	k_4	K_i	v_B
A	HCC	0.51 ± 0.16		0.43 ± 0.16	0.03 ± 0.02	0.01 ± 0.01	0.02 ± 0.02	0.02 ± 0.02
	Remote	0.64 ± 0.15		0.47 ± 0.13	0.002 ± 0.006	0.01 ± 0.02	0.01 ± 0.03	0.01 ± 0.03
	t-test	*0.02*		0.71	*< 0.01*	0.63	*< 0.01*	0.6
B	HCC	0.16 ± 0.51	1.42 ± 0.84	1.04 ± 0.41	0.04 ± 0.03	0.004 ± 0.005	0.04 ± 0.02	0.13 ± 0.06
	Remote	0.13 ± 0.20	2.19 ± 1.81	1.20 ± 1.06	0.001 ± 0.001	0.001 ± 0.002	0.00 ± 0.00	0.10 ± 0.05
	t-test	0.80	0.25	0.73	*< 0.01*	*0.02*	*< 0.01*	0.2
C	HCC		2.37 ± 1.46	1.35 ± 0.76	0.03 ± 0.03	0.003 ± 0.004	0.04 ± 0.04	0.25 ± 0.16
	remote		3.77 ± 2.46	1.75 ± 1.33	0.001 ± 0.001	0.001 ± 0.001	0.001 ± 0.001	0.14 ± 0.24
	t-test		*0.04*	0.07	*< 0.01*	*0.02*	*< 0.01*	*0.01*
Wang		K_1	k_2	k_3	k_4	f_A	k_A	K_i
	HCC	1.95 ± 1.86	0.82 ± 0.73	0.05 ± 0.03	0.01 ± 0.02	0.17 ± 0.11	1.94 ± 1.48	0.11 ± 0.09
	Remote	1.90 ± 1.87	1.62 ± 0.90	0.17 ± 0.19	0.25 ± 0.28	0.14 ± 0.06	1.44 ± 0.77	0.10 ± 0.11
	t-test	0.78	*0.01*	*0.02*	*< 0.01*	0.48	0.33	0.71

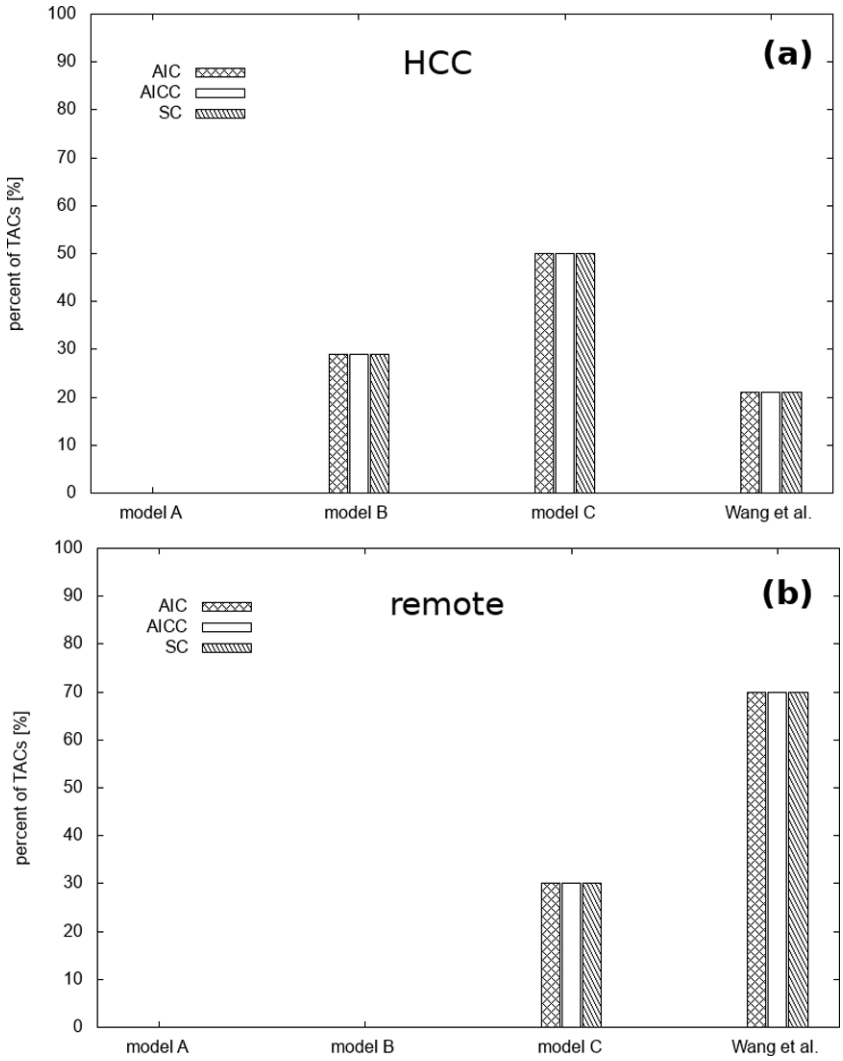

Figure 3. Percentage of the TACs showing a preference for a certain criterion, for hepatocellular carcinoma regions (HCC) and healthy liver regions (remote). AIC: Akaike Information Criterion; AICC: unbiased Akaike Information Criterion (AICC); SC: Schwartz Criterion.

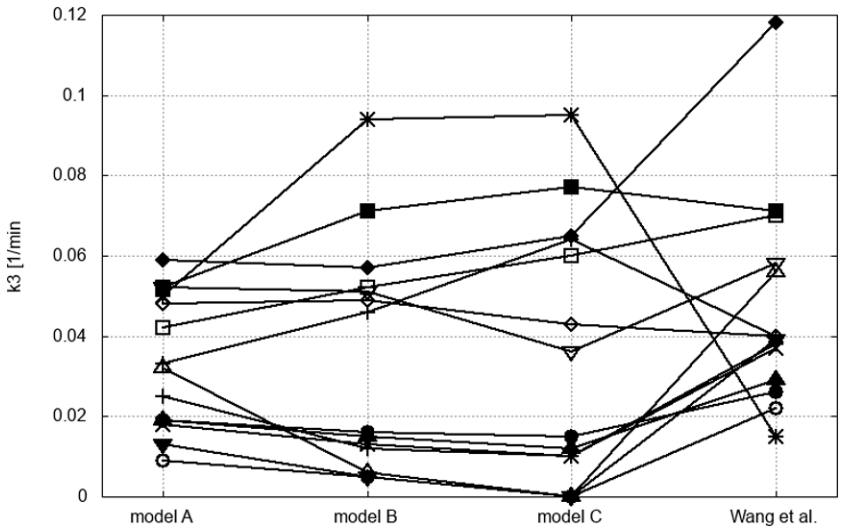

Figure 4. Value of k_3 after fitting the time concentration curves with each model (model A, model B, model C and Wang's model), shown for all 14 measured HCC regions.

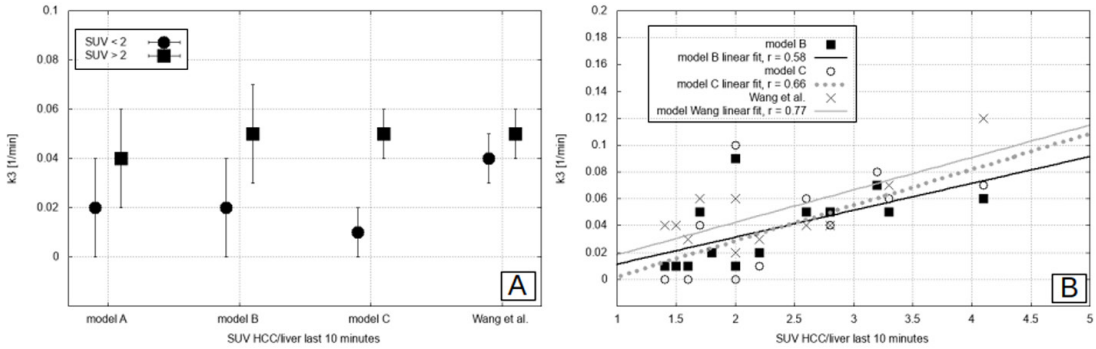

Figure 5. (A) averaged k_3 of all hepatocellular carcinoma regions (HCC) separated into one group with HCC to liver ratio (calculated from the last 10 min of the scan) of <2 (circles, $n = 8$) and one group with $\geqslant 2$ (rectangles, $n = 8$). (B) Correlation of k_3 with HCC/liver ratio, including a line of best fit and the correlation coefficient r for each model. For the sake of visibility, only the three most relevant models are shown.

As already declared in many different ways (Munk *et al* 2001, Cui and Bai 2005, Keiding 2012), using solely the hepatic artery as input function is not sufficient to describe FDG processes in the liver. We could confirm this with Model A which turned out to be the least preferred model according to all criterion tests. Wang's model, although using the highest number of fit parameters, is still preferred for remote region. Unexpectedly, it has the least significant differences between HCC and remote TACs.

While other studies performed with different tracers, modalities or diseases (Chen *et al* 2013, Wang *et al* 2018) suggest a main contribution of the hepatic artery to blood supply in the liver, in our case the preferred model for HCC regions is model C, using solely the portal vein as input function. While all models showed significant differences in K_v and k_3 between HCC and remote TACs, only model C also has significant differences in v_B, indicating that both regions are supplied with different intensity with blood. Certainly, the differences in model C between HCC and remote regions in the parameters k_3 and K_i are probably not significant due to different tracer kinetics but due to the fact that model C is clearly not ideal for describing the remote region (see figure 3(b)). Therefore, model C might not be applicable to quantify remote region, but more to differentiate between healthy and HCC regions.

The obtained values for v_B with all models except model A are in good agreement with values obtained with blood sample measurements as input function (Hays and Segall 1999). In model B, even more preferred than Wang's model, v_B is naturally lower compared to model C due to the shape of the portal vein TAC. In this model, the variability of K_A and K_V was between 0.00 min^{-1} and 0.62 min^{-1}, and between 0.07 min^{-1} and 3.04 min^{-1}, respectively, for HCC regions. Note that for only six HCC TACs, K_A was greater than 0.1 min^{-1}, which in contrary showed very high K_V values of greater than 1. This supports the idea that most of the HCC regions are mainly supported by solely one input function, namely with higher probability by the portal vein and with lower probability by the hepatic artery.

Interestingly, we could observe similar values of k_3 and K_i within models A, B and C, which gave values for k_3 of around 0.03 min^{-1} for HCC TACs, and values of almost zero for k_3 and k_4 in case of remote TACs. This was vice versa in case of Wang's model, where HCC k_3 and k_4 were slightly higher compared to the other models but significantly higher for remote TACs. In Wang's study itself, similar values for non-remote k_3 and k_4 were published, although only nonalcoholic fatty liver disease was studied and not HCC. Since Wang's model is clearly preferred in case of remote TACs showing very different values for k_3 and k_4, one can conclude that (1) it is not advisable to use the same model for both, HCC and remote tissue, and that (2) therefore phosphorylation and thus metabolism is slower in HCC tissue.

Concerning high values for remote regions, also slightly different results were obtained by Salem *et al* (2007) who used blood sample measurements for arterial input and an image derived portal vein for venous input in a model similar to our model B on HCC as well as remote region of rodents. While their model is different and therefore does not allow a comparison with K_a and K_v, their values for v_B and k_2 are comparable with our values. Also k_3 was higher in case of HCC compared to remote TACs. However, k_3 and k_4 were in general higher compared to our values with averaged 0.12 ml min^{-1} and 0.3 ml min^{-1}, respectively, for HCC and 0.07 ml min^{-1} and 0.3 ml min^{-1}, respectively, for remote TACs. Also in accordance with Salem *et al* (2007), k_3 was significantly lower in HCC regions showing a low HCC-to-remote ratio (<2).

Limitations

Due to a missing partial volume and motion correction, the measured input functions are lowered, leading to unrealistically high values for K_a, K_v and k_2 which therefore cannot be taken as an absolute quantification. Since the size of the volumes of all HCC regions are—with one exception—higher than 3 cm^3, partial volume effects might be neglected for HCC. For the input functions, partial volume and motion effects are not negligible. In contrary to Huo *et al* (2015), we intentionally did not take the arterial input function from the aorta but from the hepatic artery, because a comparison of one- and dual-input-function models appears more meaningful assuming that these effects are more similar between portal vein and hepatic artery. Although we intended to study the impact of different input functions, partial volume effects nevertheless could lead to a false model preference. However, the applied criteria tend to select models with less parameters, which is clearly not the case for the remote TACs. Assuming also similar fluctuations in remote and HCC TACs, we thus conclude that partial volume effects have a minor impact on the model preference. Furthermore, taking the maximum SUV values of HCC relative to remote (table 1) as measure for the severeness of partial volume and motion effects, these effects are below 20% in case of hepatic artery and below 30% in case of portal vein, which is much lower than the differences between HCC and remote region or between group 1 and group 2. A further limitation might be the lack of clinical parameters. We therefore used an SUV threshold as a classification outline for lesions to assess whether k_3 is in general suitable for tumor classification.

Conclusion

We could show that a simple two-tissue model using solely the portal vein is sufficient to differentiate HCC from liver tissues. It might be necessary to apply different models for HCC and healthy liver tissue, whereas for healthy tissue models using a dual input function approach is preferred. The values of k_3 and K_i were almost identical between all models. k_3 showed significant differences between remote and HCC regions as well as between different classes of HCC concerning their SUV.

Acknowledgments

Conflicts of interest and Sources of funding: Supported by the National Natural Science Foundation of China 36 (Grant No. 81571713, 81671722), CAMS Innovation Fund for Medical Sciences (CIFMS) (Grant No. 2016-37 I2M-4-003), CAMS Initiative for Innovative Medicine (Grant No. CAMS-2018-I2M-3-001). None declared to all 11 authors.

References

Akinyemiju T *et al* (Global Burden of Disease Liver Cancer Collaboration) 2017 The burden of primary liver cancer and underlying etiologies from 1990 to 2015 at the global, regional, and national level: results from the global burden of disease study 2015 *JAMA Oncol.* **3** 1683–91

Chen K *et al* 1998 Noninvasive quantification of the cerebral metabolic rate for glucose using positron emission tomography, ^{18}F-fluoro-2-deoxyglucose, the Patlak method, and an image-derived input function *J. Cereb. Blood Flow Metab.* **18** 716–23

Chen Y W *et al* 2013 Assessment of blood flow in hepatocellular carcinoma: correlations of computed tomography perfusion imaging and circulating angiogenic factors *Int. J. Mol. Sci.* **14** 17536–52

Cui Y and Bai J 2005 Comparison of parameter estimations using dual-input and arterial-input in liver kinetic studies of FDG metabolism *Conf. Proc. IEEE Engineering in Medicine and Biology Society* vol 3 pp 2345–8
El Dika I, Khalil D N and Abou-Alfa G K 2019 Immune checkpoint inhibitors for hepatocellular carcinoma *Cancer* **125** 3312–9
Galle P R *et al* 2018 EASL clinical practice guidelines: management of hepatocellular carcinoma *J. Hepatol.* **69** 182–236
Geist B K *et al* 2018 Assessing the kidney function parameters glomerular filtration rate and effective renal plasma flow with dynamic FDG-PET/MRI in healthy subjects *EJNMMI Res.* **8** 37
Golla S S V *et al* 2017 Model selection criteria for dynamic brain PET studies *EJNMMI Phys.* **4** 30
Hays M T and Segall G M 1999 A mathematical model for the distribution of fluorodeoxyglucose in humans *J. Nucl. Med.* **40** 1358–66
Heimbach J K *et al* 2018 AASLD guidelines for the treatment of hepatocellular carcinoma *Hepatology* **67** 358–80
Ho C L, Yu S C and Yeung D W 2003 ^{11}C-acetate PET imaging in hepatocellular carcinoma and other liver masses *J. Nucl. Med.* **44** 213–21
Huo L *et al* 2015 Kinetic analysis of dynamic (11)C-acetate PET/CT imaging as a potential method for differentiation of hepatocellular carcinoma and benign liver lesions *Theranostics* **5** 371–7
Huo L *et al* 2018 Performance evaluation of a new high-sensitivity time-of-flight clinical PET/CT system *EJNMMI Phys.* **5** 29
Keiding S 2012 Bringing physiology into PET of the liver *J. Nucl. Med.* **53** 425–33
Kudomi N *et al* 2009 Non-invasive estimation of hepatic glucose uptake from [18F]FDG PET images using tissue-derived input functions *Eur. J. Nucl. Med. Mol. Imaging* **36** 2014–26
Lee S M, Kim H S, Lee S and Lee J W 2019 Emerging role of (18)F-fluorodeoxyglucose positron emission tomography for guiding management of hepatocellular carcinoma *World J. Gastroenterol.* **25** 1289–306
Li S *et al* 2017 The value of [(11)C]-acetate PET and [(18)F]-FDG PET in hepatocellular carcinoma before and after treatment with transarterial chemoembolization and bevacizumab *Eur. J. Nucl. Med. Mol. Imaging* **44** 1732–41
Margini C and Dufour J F 2016 The story of HCC in NAFLD: from epidemiology, across pathogenesis, to prevention and treatment *Liver Int.* **36** 317–24
Munk O L, Bass L, Roelsgaard K, Bender D, Hansen S B and Keiding S 2001 Liver kinetics of glucose analogs measured in pigs by PET: importance of dual-input blood sampling *J. Nucl. Med.* **42** 795–801
Okazumi S *et al* 1992 Evaluation of liver tumors using fluorine-18-fluorodeoxyglucose PET: characterization of tumor and assessment of effect of treatment *J. Nucl. Med.* **33** 333–9
Salem N *et al* 2007 Quantitative evaluation of 2-deoxy-2[F-18]fluoro-D-glucose-positron emission tomography imaging on the woodchuck model of hepatocellular carcinoma with histological correlation *Mol. Imaging Biol.* **9** 135–43
Schmidt K C and Turkheimer F E 2002 Kinetic modeling in positron emission tomography *Q. J. Nucl. Med.* **46** 70–85
Siegel R L, Miller K D and Jemal A 2018 Cancer statistics *CA Cancer J. Clin.* **68** 7–30
Wang G, Corwin M T, Olson K A, Badawi R D and Sarkar S 2018 Dynamic PET of human liver inflammation: impact of kinetic modeling with optimization-derived dual-blood input function *Phys. Med. Biol.* **63** 155004